Magnetic correlations and crystal structure changes in Fe and Ni substituted $ErCo_2$ with reversible giant magnetocaloric effect

Simon Rosenqvist Larsen,* Noriki Terada,† Xin Tang, and Hiroaki Mamiya

Research Center for Magnetic and Spintronic Materials,
National Institute for Materials Science, 1-2-1,
Sengen, Tsukuba, Ibaraki, 305-0047, Japan

Yusuke Nambu

Institute for Materials Research, Tohoku University, Sendai, Miyagi 980-8577, Japan
Organization for Advanced Studies, Tohoku University,
Sendai, Miyagi 980-8577, Japan and
FOREST, Japan Science and Technology Agency,
Kawaguchi, Saitama 332-0012, Japan

Daisuke Okuyama

Institute of Materials Structure Science,
High Energy Accelerator Research Organization,
Oho 1-1, Tsukuba, Ibaraki 305-0801, Japan

Hossein Sepehri-Amin

Research Center for Magnetic and Spintronic Materials,
National Institute for Materials Science, 1-2-1,
Sengen, Tsukuba, Ibaraki, 305-0047, Japan and
Institute of Engineering Science, University of Tsukuba,
1-1-1 Tennodai, Tsukuba, Ibaraki, 305-8573 Japan

Abstract

$ErCo_2$ is a compound which has recently garnered attention as a potential applicable magnetic refrigeration material for hydrogen liquefaction. The interest in the material is due to the large magnetocaloric effect it exhibits, the tunability of the transition temperature, and the recent discovery of the tunability of the order of the transition by small substitutions of transition metals. (Tang et. al. Nat. Commun. 13, 1817 (2022)) The reason for the change in the order of the transition is not yet understood. In this study the microscopic magnetic correlations and crystal lattice distortions in $ErCo_{2-x}T_x$ (T=Fe and Ni) are investigated by neutron and synchrotron X-ray diffraction, as well as AC susceptibility measurements. The results indicated that in contrast to the previous study, the cubic to rhombohedral structure change was not suppressed, though the way the unit cell expansion occurred did change. No significant changes were observed in the magnetic long range order and crystal lattice symmetry, which still formed a ferrimagnetic and rhombohedral crystal structure below the phase transition temperature (T_C) for all substitutions as well as pure $ErCo_2$. However, an increase in magnetic short range correlations above T_C, which is strongly correlated with the entropy change and the dynamic AC susceptibility, was detected only in the substituted samples. Unlike pure $ErCo_2$, the nucleation of the local ferrimagnetic clusters above T_C occurs in the substituted samples, which significantly reduces the energy barrier between the higher temperature cubic phase and the lower temperature rhombohedral phase. It is concluded that the reduction of the energy barrier due to the development of short range order induced by chemical substitution at temperatures above T_C is possibly the origin of the significant change in the nature of the phase transition in $ErCo_2$.

I. INTRODUCTION

The magnetocaloric effect has been identified as a potential way of significantly reducing energy consumption for cooling applications. Recently there has been an increased focus on creating materials for hydrogen liquefaction. This is due to hydrogen being positioned to be the main energy carrier in the energy infrastructure of society in the future. Hydrogen is being positioned for this purpose due to it possessing a very high energy density per mass

* larsen.simon@nims.go.jp

† terada.noriki@nims.go.jp

compared to other energy carriers [1]. However, hydrogen is gaseous under the ambient conditions of earth and has low mass density, and in order for it to be transported for use it is desirable to keep it in the liquid state. Hydrogen needs to be cooled to 20 K in order for it to condense, and while the cooling from room temperature to 77 K can be done cheaply using liquid nitrogen, the remaining temperature range from 77 K to 20 K is difficult and expensive. Magnetocaloric materials covering this temperature range would significantly reduce the energy cost of cooling [2].

There are several properties of materials that need to be considered when investigating them for use as magnetocaloric materials. Chief among these properties is the entropy change when applying a magnetic field, which defines if the material can be used for magnetic cooling. The entropy change can have various origins, though it typically occurs when a magnetic transition, a structural transition, or the simultaneous transition of both happens. As a result, these transitions and the temperature ranges they occur in significantly impact the magnetocaloric properties of the materials. First order transitions exhibit the largest entropy changes, but suffer from hysteresis which hinders reversibility, shifts the operational temperature range, and lowers the entropy change upon further cycling. Second order transitions do not suffer the same issue, but have smaller changes in entropy. A material with a hysteresis-free second order transition with a large entropy change would therefore be highly desirable for applications. There are many effects, both extrinsic and intrinsic, which influence the hysteresis, and understanding the origin of it is necessary to define the scope of future engineering of the material [3].

Many materials such as $GdCo_2B_2$ [4] and HoB_2 [5], are being investigated for use as the main components in a magnetocaloric cooling cycle for hydrogen liquefaction. One of the most intriguing of these materials is the $ErCo_2$ based system. While this particular material has been known for having a strong first order magnetocaloric transition for some time [6], it was recently discovered that a series of small substitutions in the system can create materials which can cover the entire operating range desired for hydrogen liquefaction [7]. In addition to successfully covering the entire temperature range needed for applications, it also intriguingly displayed a marked shift from a first order transition to a second order transition without experiencing a large loss in entropy change. The magnetic transition in $ErCo_2$, which typically occurs around 35 K, is composed of a simultaneous magnetic and structural transition where the cubic paramagnetic phase elongates in the (111) direction

and transforms into a ferrimagnetic rhombohedral structure [8]. In this configuration the large Er moments align along the rhombohedral c-axis (in the hexagonal setting) while the smaller Co moments align oppositely. The structural transition was reported as being suppressed when substitutions were added, which was suggested as the cause in the change of the order of the transition. While the suppression of the structural transition is likely an important feature for the reduction of the hysteresis, the role that the magnetic interactions play in this case was not considered [7]. Thus, the goal of this study is to understand what impact the magnetic interactions have on the hysteresis in $ErCo_2$. To accomplish this the static and dynamics spin correlations and magnetostructural distortions are investigated by using neutron diffraction, X-ray diffraction and AC susceptibility measurements.

II. EXPERIMENTAL DETAILS

Polycrystalline samples of $ErCo_2$, $ErCo_{1.96}Fe_{0.04}$, $ErCo_{1.95}Fe_{0.05}$, and $ErCo_{1.80}Ni_{0.20}$ were synthesized by melting stoichiometric amounts of Er (99.9%), Co (99.97%), Fe (99.99%), and Ni (99.95%) together in an arc furnace under Ar atmosphere. To compensate for material loss due to evaporation, 2-5wt.% of excess Er was added during synthesis. The samples were flipped and remelted four times to promote homogeneity. The samples were subsequently sealed in quartz glass ampules under Ar atmosphere and annealed at 1273 K for 50 h before being manually ground to a powder by pestle and mortar using acetone as a grinding medium. All samples contained trace amounts of two oxides, Er_2O_3, and a Pr_7O_{12} based structure [9] which likely consisted of Er and O and stabilized by the presence of a small amount of Co. The Fe substituted samples also contained the $ErCo_3$ impurity phase. It should be noted that $ErCo_3$ seems to be unevenly distributed in the samples even after annealing, as different amounts of $ErCo_3$ have been observed in different parts of the sample using X-ray diffraction and SEM measurements (see supplementary Fig. 1 [10]). As neutron diffraction requires large amounts of sample, and the fact that $ErCo_3$ is magnetic when paramagnetic measurements were done for the $ErCo_2$, its contribution is likely seen more in these measurements. Despite the presence of the impurity phase, the behavior of the unit cell parameters observed by synchrotron diffraction were consistent, even with clear differences in $ErCo_3$ content. The results were also in line with previous studies that did not detect $ErCo_3$ such as [7] and [11], suggesting that the impurity phase does not play as large

a role. Furthermore, $ErCo_3$ was clearly detected in [12] but exhibited similar susceptibility to [13], where the impurity phase was not detected.

Low-magnification Scanning Electron Microscopy with Energy-Dispersive X-ray Spectroscopy (SEM-EDS) analysis was performed using a scanning electron microscope (SEM, Carl Zeiss CrossBeam 1540EsB) after mechanical surface polishing.

Neutron powder diffraction (NPD) experiments were carried out at the HERMES beamline at JRR-3 reactor source in Tokai, Japan [14]. The incident neutron wavelength was measured by a LaB_6 standard to be $\lambda = 2.19704$ Å. Scans were collected at temperatures between 250 and 2 K for the various samples, with the low temperatures being achieved through the use of a closed-cycle He refrigerator.

Synchrotron X-Ray powder diffraction (XRPD) experiments were carried out at BL-8A at the Photon Factory facility in Tsukuba, Japan. The samples were mounted in sealed glass capillaries, and data was collected using a large cylindrical imaging plate. A CeO_2 standard was used to measure the wavelength which was found to be $\lambda = 0.689088$ Å. A He gas-flow cryostat was used to enable temperature measurements from just below room temperature and down to approximately 25 K.

AC susceptibility measurements were conducted on a Physical Property Measurement System made by Quantum Design. Powder samples of masses around 10 mg were measured in a temperature range of 10-290 K with frequencies of 10, 56, and 316 Hz. In addition to measurements under no applied field, scans were also conducted with applied fields of 0.1, 0.5, 1.0, 3.0 and 5.0 T.

III. RESULTS

A. Magnetic correlations

1. Neutron diffraction

Neutron diffraction patterns of the paramagnetic state were collected at 100 K for $ErCo_2$ and 250 K for all other samples. Figure 1 shows the neutron diffraction patterns and Rietveld refinements of $ErCo_2$, $ErCo_{1.96}Fe_{0.04}$, $ErCo_{1.95}Fe_{0.05}$, and $ErCo_{1.80}Ni_{0.20}$ in the paramagnetic phase. The model refinements indicated that $ErCo_2$ and $ErCo_{1.80}Ni_{0.20}$ formed a single phase of the cubic $MgCu_2$-type Laves phase. In the Fe substituted samples $ErCo_{1.96}Fe_{0.04}$

and $ErCo_{1.95}Fe_{0.05}$, additional reflections were present which could be modeled with $ErCo_3$, a $PuNi_3$-type rhombohedral structure. The $PuNi_3$-type and the $MgCu_2$-type Laves phase are related through the $CaCu_5$-type structure [15]. The five atoms making up the unit cell in $ErCo_3$ form a ferrimagnetic structure which persists up to 401 K [16]. In the refinements where $ErCo_3$ was present, the magnetic structure of the system is included with moments fixed to values extracted from previous studies of the compound [16, 17].

The magnetic long range ordered structure was for all samples found to be the rhombohedrally distorted cubic structure, with a ferrimagnetic structure where Er moments align along the c-axis of the hexagonal setting of the rhombohedral structure, and with the Co moments aligned oppositely [8]. In the rhombohedral structure the Co is on the $3b$ and $9e$ sites of space group $R\bar{3}m$, and the magnetic moment size of these can be individually refined, however they almost always converged to the same values within the experimental accuracy and, due to the instability of some refinements, were fixed to refine to the same value. Neutron diffraction patterns and model refinements are presented in Fig. 2, with the refinement parameters displayed in Table I. A visualization of the magnetic structure is presented in Fig. 3(a), while the size of the Er and Co moments are displayed in Figs. 3(b) and 3(c) respectively. The ferrimagnetic nature is in agreement with previous reports on $ErCo_2$, however the Er moment sizes uncovered here of around 7.9 ± 0.1 μ_B, is lower than the values of around 9 μ_B reported in the other studies [8, 18–22]. This discrepancy could potentially be explained by the low resolution of neutron diffraction data preventing the rhombohedral distortion being noticed, causing differences in analysis due to the system being treated as the cubic $MgCu_2$-type instead. On the other hand the study which did successfully identify the rhombohedral structure [8] found the Er moment to be 8.8 μ_B, supporting the case for larger moments than what is presented here. In contrast, the Co moment was consistently seen to be 1.0 μ_B in temperatures ranging from 4.2 K to 30 K, agreeing with the other reports [18–21]. Measurements of the saturation magnetization, which can be seen in supplementary Fig. 2 [10], indicated a saturated value of approximately 6.5 μ_B/f.u. at 6 T, which when subtracting the neutron model values of the Co moment of 1.0 μ_B from the Er moment of 7.9 μ_B, is close to the value, 5.9 μ_B/f.u., estimated in the ferrimagnetic arrangement from the neutron diffraction experiment. Similar values have also been observed in Er deficient systems [12].

It is clear that substitutions do not impact the magnetic structure significantly, with all

samples attaining the same structure type but with a slight decrease in magnetic moment size as the amount substituted increased. The other distinguishing feature between the samples is the more gradual increase in moment in the substituted samples compared to the base $ErCo_2$. Below T_C, the gradual increase in intensity of the main magnetic reflection of *101* and *003* at around 30° seen in supplementary Fig. 3 [10], with the integrated in Fig. 4(a), show very similar features to the moment values estimated from the Rietveld refinements. This indicates that the gradual increase but higher temperature for the onset of order observed in the Fe substituted samples is indeed present.

Diffuse scattering related to short range order was observed in the low scattering region of 2-10 ° in the diffraction data. The intensity of the diffuse component was comparable to some main Bragg reflections. The intensity increased upon cooling until it reached the T_C of the sample, after which it rapidly decreased as the long range order was established. The temperature dependence of this short range order was evaluated by integrating the region from the lowest angle up to the angle where the intensity is stable around the background intensity level. This region spans from 2 to 13.5 ° in 2θ, and a visualization of the intensity in this region for the various samples can be seen in Fig. 5. When integrating the low angle region differences were observed in the relative intensities for the Ni substituted samples compared to the other samples, as seen in Fig. 4(b). The intensity at low scattering angles is generally associated with ferromagnetic short range order, and the increase just above T_C is a typical feature. The similar curves for $ErCo_2$ and Fe substituted samples suggests the behavior of the moments between these samples does not change significantly as T_C is approached. It should be noted that while the temperature dependence of the diffuse intensity of the samples is somewhat similar, there is a slight shift in the temperature where the maximum shows. While the intensities are small enough to be within uncertainty, the entropy change observed in a previous study [7] shows a maximum coinciding with the associated temperatures. This suggests that the short range ordering plays an important role in the magnetocaloric effect in the system. The large amount of intensity seen for the $ErCo_{1.80}Ni_{0.20}$ would indicate a large amount of short range correlations or spin fluctuations.

To better understand the differences in how the short range correlations behave in the system, the correlation length was sought determined. This has previously been done for $ErCo_2$ in the small angle diffraction region using the Ornstein-Zernike formula to study magnetic clusters [23]. By fitting the 2 to 13.5 ° in 2θ region (0.10 to 0.67 $Å^{-1}$ in Q) with

this formula, the correlation length at different temperatures can be extracted, as seen in Fig. 6. $ErCo_2$ and $ErCo_{1.80}Ni_{0.20}$ exhibit a stable, or slightly decreasing correlation length of 5-7 Åbefore the onset of long range order, which is consistent with the previous report on the system [23]. The correlation lengths of $ErCo_{1.96}Fe_{0.04}$ and $ErCo_{1.95}Fe_{0.05}$ instead increases to 9-11 Åas the temperature increases. The increase of the correlation lengths at very low substitutions of Fe would suggest that the Fe atoms serve as a sort of nucleation point for the magnetic clusters, and allowing them to grow larger than in $ErCo_2$.

2. AC susceptibility

The neutron data hinted to the presence of a large amount of short range order just above T_C which can be connected to magnetocaloric effect in the system. In order to investigate the dynamics for the observed short range order in the neutron diffraction data, AC susceptibility measurements were conducted on the samples, the results of which can be seen in Fig. 7. There are several intriguing differences between the base $ErCo_2$ sample and the substituted samples worth noting. Beginning with the case of no applied external field, it is clear that the real part of the susceptibility, χ'_{ac}, exhibits a maximum near the expected transition temperatures, but $ErCo_{1.95}Fe_{0.05}$ and $ErCo_{1.80}Ni_{0.20}$ have much larger and broader signals than $ErCo_2$. The broad signals of $ErCo_{1.95}Fe_{0.05}$ and $ErCo_{1.80}Ni_{0.20}$ extend well above T_C and is indicative of more short range order in these compounds. The broadening has previously been observed for Er-deficient samples, and the largest intensity increase seems to be tied to this broadening as well [12, 13]. The change in the magnetic properties in these systems has in one case been attributed to the molecular field being altered [13], and in the other case to the appearance of the $ErCo_3$ impurity phase [12]. Considering the Ni substituted sample, which did not contain $ErCo_3$, is also broadened, it seems more reasonable that changes to the molecular field are the origin of this feature. The imaginary component χ''_{ac} also has significant differences between the samples. $ErCo_2$ shows a sharp transition at T_C, while the substituted samples exhibit a broad peak above T_C, with the maximum at temperatures where the diffuse scattering intensity also peaks. This suggests that the energy dissipation occurs as the magnetic short range order grows. AC susceptibility measurements were conducted at other frequencies, however no significant differences were observed as can be seen in supplementary Fig. 4 [10].

Applying an external field promotes magnetization in each domain aligned along the field direction, which would change the domain wall dynamics giving insight into the role they play in the systems. Both χ''_{ac} peaks observed in $ErCo_2$ are heavily suppressed under a field of 1 T, and completely suppressed at 3 and 5 T, indicating the formation of a single aligned domain. $ErCo_{1.80}Ni_{0.20}$ saw the wide double peak collapsing to a single one at a field of 0.1 T, before being suppressed in much the same way as $ErCo_2$.

The two peaks around T_C, with different field dependence, which compose the transition region can be attributed to two different effects. The higher temperature peak occurs above T_C just prior to the onset of long range order, and is thus associated with a large amount of local short range order, which aligns with the increased intensity seen in the low angle part of the neutron diffuse scattering. The lower temperature peak occurs after long range order has been established and likely corresponds to the movement of ferrimagnetic domain walls. The results suggest that domain wall movements are plentiful in $ErCo_2$ but sensitive to outside stimuli, whereas the addition of Fe has a stabilizing effect on the amount of domain wall movements. This could potentially arise from a distribution of local inhomogeneities in the band structure caused by Fe, resulting in a series of domain wall movements. It is also possible that the domain walls are pinned by Fe-induced impurities restraining their movement.

The dynamic susceptibility has previously been used to provide strong evidence for the existence of the Griffiths phase in $ErCo_2$, which is present around 100 K [13, 24]. While this feature is absent in the data presented here, the presence of it may be sample dependent as another study also did not observe it [12].

B. Crystal structure changes

To gain a better understanding of the effect the substitutions have on the rhombohedral configuration, measurements were conducted using in-situ synchrotron X-ray diffraction measurements. When the samples were cooled below T_C peak splitting consistent with a transition from the cubic to the rhombohedral Laves phase [25] was observed, as shown in Figs. 8(a) and 8(b). However, because of experimental limitations on the X-ray diffraction equipment, it was not possible to cool below the T_C for $ErCo_{1.80}Ni_{0.20}$. Nevertheless, the Ni containing sample still shows broadening in the NPD data of Fig. 9.

The unit cell parameters extracted from model refinements of the XRPD data are presented in Table II, and compared to the cubic values in Figs. 8(c) and 8(d). The values fall within the range of previously observed values of 7.135 Å [26] and 7.1591 Å [27], but are smaller than the typical reported values of around 7.156 Å [13, 28–30]. The values are in excellent agreement with reports on Er deficient compounds [12, 13], though no vacancies could be detected. Furthermore, the behavior of the size of the unit cell with substitutions is in line with what is expected from the transition metal atomic sizes. This suggests that while vacancies might be created from the formation of impurity phases, this does not influence the unit cell parameters as much as the transition metals.

It is interesting to note the differing expansion of the unit cell between the samples seen in Figs. 8(c) and 8(d). This difference is consistent across pure Fe and Co based systems with the Fe samples favoring the larger a-axis expansion as seen in the original rhombohedral Laves phase, $TbFe_2$ [25], and $SmFe_2$ [31], while the Co prefers a larger c-axis as seen for $TbCo_2$ [32–34]. The expansion observed here is also in agreement with the previous report on $ErCo_2$ and Fe substitutions [7].

The unit cell volume per formula unit in the temperature region near the cubic to rhombohedral transition is displayed in Fig 10. A clear change in volume is observed for the Fe-substituted sample as well as $ErCo_2$, which conflicts with the previous report on the substituted system [7]. This discrepancy likely arose due to the use of low resolution laboratory X-ray measurements in the previous report, making it difficult to assess the unit cell changes compared to synchrotron data.

IV. DISCUSSION

By combining all the experimental results, it is possible to understand the underlying mechanism behind the changes in the nature of the first order phase transition in transition metal substituted $ErCo_2$. Previous studies of Co based Laves compounds have demonstrated that Co in these systems shows Pauli-paramagnetic behavior with non-polarized band structure without the presence of an external field or an internal molecular field. When above T_C in $ErCo_2$, the molecular field created by the paramagnetic Er magnetic moments locally induce small amounts of Co moments, as illustrated in Fig. 11(a). The size of the Co moment has been reported to be approximately 0.2 μ_B [23]. Decreasing the temperature below

T_C leads to the first order cubic to rhombohedral phase transition, which occurs in order for the system to gain magnetic exchange interaction energy, and simultaneously realizes the polarized band structure state of Co (Fig. 11(b)). In pure $ErCo_2$ with no chemical disorder, the discontinuous first order phase transition with hysteresis occurs due to the existence of an energy barrier between the paramagnetic cubic state and the ferrimagnetic rhombohedral state.

In the case of Fe-doped systems, unlike the pure $ErCo_2$, short range order appears over a wide temperature range above T_C (50 K < T < 80 K (in $ErCo_{1.95}Fe_{0.05}$ case) as was observed in both the neutron diffraction and χ_{ac} data. Considering previous studies of pure $ErFe_2$ [35], it is expected that the 3d electrons band structure is highly polarized (the magnetic moment of Fe is 1.97 μ_B in $ErFe_2$), even for Fe atoms in $ErCo_2$. For temperatures well above T_C, Er and Co spins are paramagnetic (Fig. 11(c)). When cooled and the temperature approaches T_C, the local ferrimagnetic coupling between Fe and Er spins start growing due to the antiferromagnetic exchange interactions between the two spins increasing (Fig. 11(d)). Co-spins can also be affected by the molecular fields created by the local ferrimagnetic ordering of Fe and Er spins. It should be noted that in this case the molecular field is not uniform but inhomogeneous due to the random distribution of Fe-atoms in the sample. The non-uniformity of the molecular field creates inhomogeneous domain states leading to the short range order observed in the neutron experiments, and high magnetic field response in the magnetic susceptibility. This is consistent with previous X-ray magnetic circular dichroism experiments which showed the magnetization of Er and Co-spins increasing in the same temperature region [7]. The nucleation of local clusters above T_C can also reduce the energy barrier between the higher temperature cubic phase with the short range order (50 K < T < 80 K) and the lower temperature rhombohedral ferrimagnetic long range order phase (T < T_C = 50 K), which is in contrast to the situation for the large energy barrier in pure $ErCo_2$. Thus it is possible that the reduction of the energy barrier due to the development of Fe substitution induced short range order at temperatures above T_C is the origin of the significant changes in the first order phase transition. This would be somewhat similar to $Er(Co_{0.875}Fe_{0.125})_2$ [11] and $Tb(Ni_{1-x}Fe_x)_2$ [36] where it was suggested that local anisotropy variations arising from Fe inclusions caused randomization of the moments of the rare-earth elements.

In the Ni substituted sample, the Ni atoms have no magnetic moment, which is expected

from the literature of $ErNi_2$ [37]. Therefore, the Ni substitutions just introduce magnetic vacancies reducing the average amount of exchange interactions leading to lowered T_C, and increased magnetic short range order. The relatively large amount of substituted transition metal (10% in the present case) in the Ni substituted sample introduces more randomness resulting in a large number of domain walls in the sample. The expected large energy dissipation in the Ni substituted sample is consistent with the relatively large broad peak observed in χ''_{ac}. Previous studies using AC susceptibility measurements also noted similar changes for Er vacancies, and attributed this to defects [13] or the impurity phase $ErCo_3$ [12]. In $ErCo_{1-x}Si_x$, it was suggested the pinning of the domain walls were caused by intrinsic defects which arose from the addition of Si [38].

The difference in the distortion of the ferrimagnetic rhombohedral structure of $ErCo_2$ and the Fe substituted samples (Figs. 8c and 8d) is an interesting feature, and it is worth considering why it arises. The additional Fe molecular field can be expected to affect the band structure of Co, schematically illustrated in Fig. 11(e). Considering the band structure is sensitive to the crystal lattice distortion in these systems, it is expected that the different type of rhombohedral distortion in Fe substituted samples is caused by changes in the band structure below T_C. Direct measurements to investigate the electronic structure such as photoelectron spectroscopy would be necessary to verify this.

V. CONCLUSIONS

In order to understand the hysteresis-free phase transition observed in Fe and Ni substituted $ErCo_2$ measured were conducted using neutron diffraction, synchrotron X-ray diffraction, and AC susceptibility. It was revealed that despite the significant change in the nature of the order of the phase transition, and previous claims of the structural transition being suppressed, the cubic $Fd\bar{3}m$ to rhombohedral $R\bar{3}m$ transition was still observed. Fe substitutions were revealed to cause a change in the direction of the expansion of the rhombohedral unit cell, as well as having a more gradual transition compared to $ErCo_2$. This did not influence the magnetic structure, however, which still attained the same rhombohedral ferrimagnetic ordering with moments aligned along the c-axis, though it did exhibit a more gradual transition for the substituted samples. Increased short range order correlations observed above T_C in the neutron data were highly correlated with the entropy change and

the AC susceptibility for the substituted samples. The nucleation of the short range clusters above T_C in the Fe-substituted samples can reduce the energy barrier between the high temperature cubic phase and the lower temperature rhombohedral phase. The origin of the change in the nature of the $ErCo_2$ phase transition by the substitutions is thus attributed to the reduction of the energy barrier which arose from the substitution induced short range order.

ACKNOWLEDGMENTS

Neutron diffraction beamtime at JRR-3 was granted through proposals 23814 and 24598, and the synchrotron x-ray diffraction beamtime at PF was granted through proposal 2023G510. This work was partially supported by the JSPS KAKENHI Grants Nos. 22H00297, JP24K00572, and JP22H05145, JST Grant No. JPMJFR202V, and the JSPS International Joint Research Program (JRP-LEAD with DFG; program number JPJSJRP20221608).

---

[1] M. Yue, H. Lambert, E. Pahon, R. Roche, S. Jemei, and D. Hissel. Hydrogen energy systems: A critical review of technologies, applications, trends and challenges. *Renewable and Sustainable Energy Reviews*, 146:111180, 2021.

[2] T. Numazawa, K. Kamiya, T. Utaki, and K. Matsumoto. Magnetic refrigerator for hydrogen liquefaction. *Cryogenics*, 62:185–192, 2014.

[3] O. Gutfleisch, T. Gottschall, M. Fries, D. Benke, I. Radulov, K.P. Skokov, H. Wende, M. Gruner, M. Acet, P. Entel, and M. Farle. Mastering hysteresis in magnetocaloric materials. *Philosophical Transactions of the Royal Society A: Mathematical, Physical and Engineering Sciences*, 374:20150308, 2016.

[4] L. Li, K. Nishimura, and H. Yamane. Giant reversible magnetocaloric effect in antiferromagnetic $GdCo_2B_2$ compound. *Applied Physics Letters*, 94:102509, 2009.

[5] P.B. de Castro, K. Terashima, T.D. Yamamoto, Z. Hou, S. Iwasaki, R. Matsumoto, S. Adachi, Y. Saito, P. Song, H. Takeya, and Y. Takano. Machine-learning-guided discovery of the gigantic magnetocaloric effect in HoB_2 near the hydrogen liquefaction temperature. *NPD*

Asia Materials, 12:35, 2020.

[6] H. Wada, S. Tomekawa, and M. Shiga. Magnetocaloric effect of $ErCo_2$. *Journal of Magnetism and Magnetic Materials*, 196-197:689–690, 1999.

[7] X. Tang, H. Sepehri-Amin, N. Terada, A. Martin-Cid, I. Kurniawan, S. Kobayashi, Y. Kotani, H. Takeya, J. Lai, Y. Matsushita, T. Ohkubo, Y. Miura, T. Nakamura, and K. Hono. Magnetic refrigeration material operating at a full temperature range required for hydrogen liquefaction. *Nature Communications*, 13:1817, 2022.

[8] J. Herrero-Albillos, F. Bartolomé, L.M. García, A.T. Young, T. Funk, J. Campo, and G.J. Cuello. Observation of a different magnetic disorder in $ErCo_2$. *Physical Review B*, 76:094409, 2007.

[9] R.E. Ferguson, E.D. Guth, and L. Eyring. Praseodymium Oxides. I. Phase Study by Dissociation Pressure Measurements. *Journal of the American Chemical Society*, 76:3890–3894, 1954.

[10] See Supplemental Material.

[11] I. Chaaba, S. Othmani, S. Haj-Khlifa, P. de Rango, D. Fruchart, W. Cheikhrouhou-Koubaa, and A. Cheikhrouhou. Magnetic and magnetocaloric properties of $Er(Co_{1-x}Fe_x)_2$ intermetallic compounds. *Journal of Magnetism and Magnetic Materials*, 439:269–276, 2017.

[12] R. Hamdi, M. Smari, A. Bajorek, L. Bessais, Y. Haik, E. Dhahri, and S. Hayek. Large magnetocaloric entropy change in ferrimagnetic $Er_{1-x}Co_2$ systems at cryogenic temperatures: the role of erbium deficiency. *Applied Physics A*, 127:39, 2021.

[13] J.D. Zou, M. Yan, and J.L. Yao. Manipulation of the magnetic properties in $Er_{1-x}Co_2$ compounds by atomic vacancies. *Journal of Alloys and Compounds*, 632:30–36, 2015.

[14] Y. Nambu, Y. Ikeda, T. Taniguchi, M. Ohkawara, M. Avdeev, and M. Fujita. Neutron Powder Diffractometer HERMES - After the Decade-Long Shutdown. *Journal of the Physical Society of Japan*, 93:091005, 2024.

[15] D.T. Cromer and C.E. Olsen. The Crystal Structures of $PuNi_3$ and $CeNi_3$. *Acta Crystallographica*, 12:689–694, 1959.

[16] R. Georges, J. Schweizer, and J. Yakinthos. Field-induced magnetic transition in $CrCo_3$. *Journal of Physics and Chemistry of Solids*, 36:415–419, 1975.

[17] E. Gratz, A.S. Markosyan, V. Paul-Boncour, A. Hoser, N.Stüsser, I.Y. Gaidukova, and V.E. Rodimin. Temperature-induced itinerant-electron metamagnetism in $ErCo_3$ studied by neu-

tron diffraction. *Applied Physics A*, 74:S698–S700, 2002.

[18] H. Oesterreicher. Magnetic and thermal studies on $ErCo_2$-$ErAl_2$. *Journal of Applied Physics*, 44:2350–2354, 1973.

[19] R.M. Moon, W.C. Koehler, and J. Farrell. Magnetic Structure of Rare-Earth-Cobalt (RCo_2) Intermetallic Compounds. *Journal of Applied Physics*, 36:978–979, 1965.

[20] H. Oesterreicher, L.M. Corliss, and J.M. Hastings. Neutron Diffraction Study of the Pseudobinary System $ErCo_2$-$ErAl_2$. *Journal of Applied Physics*, 41:2326–2330, 1970.

[21] A. Pirogov, A. Podlesnyak, T. Strässle, A. Mirmelstein, A. Teplykh, D. Morozov, and A. Yermakov. Neutron-diffraction investigation of the metamagnetic transition in $ErCo_2$. *Applied Physics A*, A74:S598–S600, 2002.

[22] A. Podlesnyak, J. Schefer, A. Furrer, A. Mirmelstein, A. Pirogov, P. Markin, and N. Baranov. Magnetic transition in $Er_{1-x}Y_xCo_2$ (x=0,0.4) single crystals probed by neutron scattering in magnetic fields. *Physical Review B*, 66:012409, 2002.

[23] J. Herrero-Albillos, D. Paudyal, F. Bartolomé, L.M. García, V.K. Pecharsky, K.A. Gschneidner, A.T. Young, N. Jaouen, and A. Rogalev. Interplay between Er and Co magnetism in $ErCo_2$. *Journal of Applied Physics*, 103:07E146, 2008.

[24] J. Herrero-Albillos, L.M. García, and F. Bartolomé. Observation of a Griffiths-like phase in the paramagnetic regime of $ErCo_2$. *Journal of Physics: Condensed Matter*, 21:216004, 2009.

[25] A.E. Dwight and C.W. Kimball. $TbFe_2$, a rhombohedral Laves phase. *Acta Crystallographica*, B30:2791–2793, 1974.

[26] D.M. Gualtieri and W.E. Wallace. Hydrogen capcity and crystallography of $ErFe_2$-based and $ErCo_2$-based ternary systems. *Journal of Less Common Metals*, 55:53–59, 1977.

[27] M. Anikin, E. Tarasov, N. Kudrevatykh, A. Inishev, M. Semkin, A. Volegov, and A. Zinin. Features of magnetic and thermal properties of $R(Co_{1-x}Fe_x)_2$, ($x \leq 0.16$) quasibinary compounds with R = Dy, Ho, Er. *Journal of Magnetism and Magnetic Materials*, 418:181–187, 2016.

[28] I.R. Harris, R.C. Mansey, M. Slanicka, and K.N.R. Taylor. Rare-earth intermediate phases. The room temperature lattice spacings of some $Gd_{1-x}Er_xCo_2$ alloys. *Journal of the Less Common Metals*, 19:437–440, 1969.

[29] M.I. Slanicka, K.N.R. Taylor, and G.J. Primavesi. Moment variation in rare earth-transition metal C15 compounds of type AFe_2-ACo_2, ACo_2-ANi_2. *Journal of Physics F: Metal Physics*,

1:679–685, 1971.

[30] B. Kotur, O. Myakush, and I. Zavaliy. Hydrogen Sorption Properties of Some $RM_{2-x}M'_x$ and $RM_{2-x}Al_x$ (R = Y, Gd, Tb, Er, Ho; M = Mn, Fe, Co, Ni) Laves Phase Ternary Compounds. *Croatica Chemica Acta*, 82:469–476, 2009.

[31] X. Liu, K. Lin, Q. Gao, H. Zhu, Q. Li, Y. Cao, Z. Liu, L. You, J. Chen, Y. Ren, R. Huang, S.H. Lapidus, and X. Xing. Structure and Phase Transformation in the Giant Magnetostriction Phase $SmFe_2$. *Inorganic Chemistry*, 57:689–694, 2018.

[32] N. Yoshimoto, J. Sakurai, and Y. Komura. X-ray diffraction study on crystal deformation of $TbCo_2$. *Journal of Magnetism and Magnetic Materials*, 31-34:137–139, 1983.

[33] Z.W. Ouyang, F.W. Wang, Q. Hang, W.F. Liu, G.Y. Liu, J.W. Lynn, J.K. Liang, and G.H. Rao. Temperature dependent neutron powder diffraction study of the Laves phase compound $TbCo_2$. *Journal of Alloys and Compounds*, 390:21–25, 2005.

[34] C. Zhou, T. Chang, Z. Dai, Y. Chen, C. Guo, Y. Matsushita, X. Ke, A. Murtaza, Y. Zhang, F. Tian, W. Zuo, Y. Chen, S. Yang, and X. Ren. Unified understanding of the first-order nature of the transition in $TbCo_2$. *Physical Review B*, 106:064409, 2022.

[35] S. Mican, D. Benea, S. Mankovsky, S. Polesya, O. Gînscă, and R. Tetean. Magnetic behaviour of $Er_{1-x}Zr_xFe_2$. *Journal of Physics: Condensed Matter*, 25:466003, 2013.

[36] N.K. Singh, K.G. Suresh, D.S. Rana, A.K. Nigam, and S.K. Malik. Role of Fe substitution on the anomalous magnetocaloric and magnetoresistance behaviour in $Tb(Ni_{1-x}Fe_x)_2$ compounds. *Journal of Physics: Condensed Matter*, 18:10775–10786, 2006.

[37] J. Ćwik, Y. Koshkid'ko, K. Nenkov, E.A. Terashima, and K. Rogacki. Structural, magnetic and magnetocaloric properties of $HoNi_2$ and $ErNi_2$ compounds ordered at low temperatures. *Journal of Alloys and Compounds*, 735:1088–1095, 2018.

[38] N.K. Singh, S.K. Tripathy, D. Banerjee, C.V. Tomy, K.G. Sureh, and A.K. Nigam. Effect of Si substitution on the magnetic and magnetocaloric properties of $ErCo_2$. *Journal of Applied Physics*, 95:6678–6680, 2004.

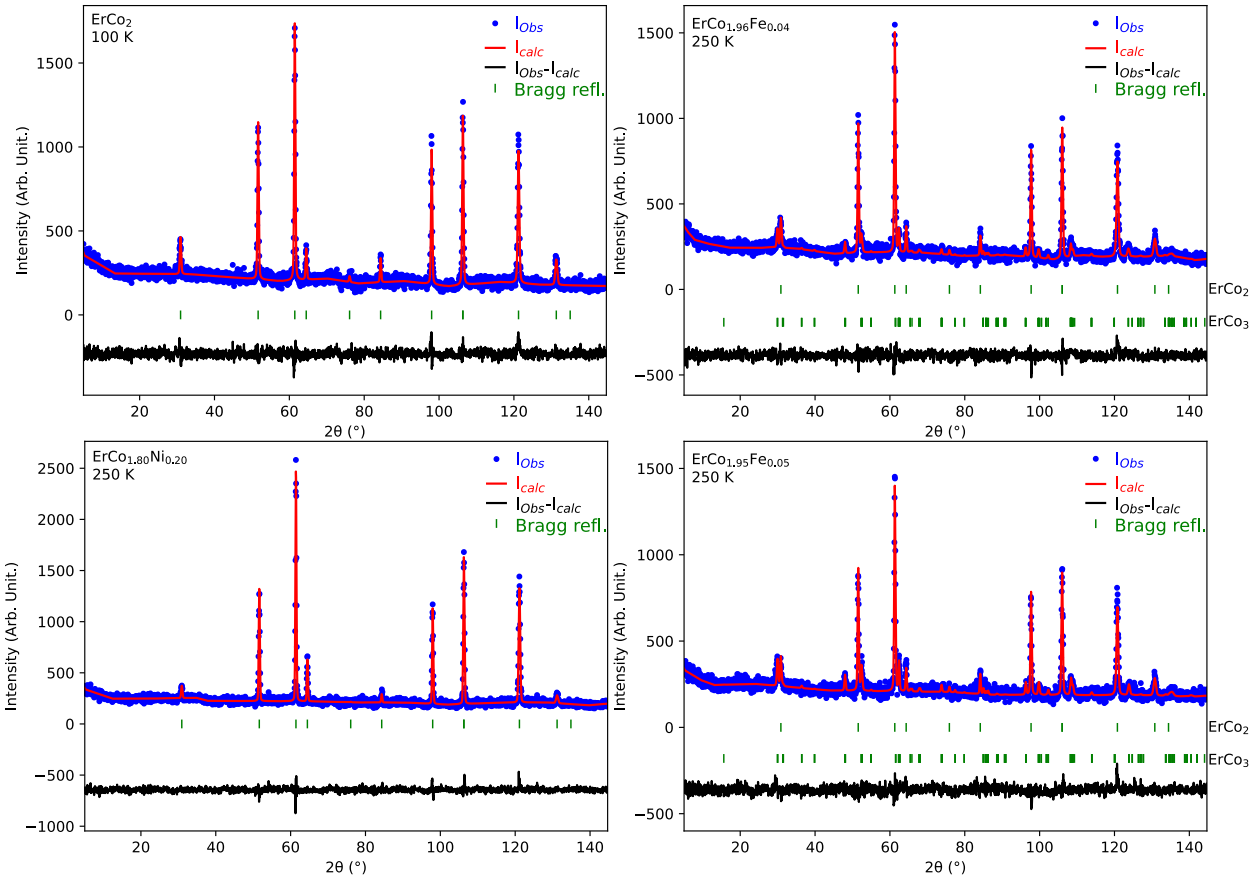

FIG. 1. Model refinements of NPD data gathered for the paramagnetic phase of $ErCo_2$, $ErCo_{1.96}Fe_{0.04}$, $ErCo_{1.95}Fe_{0.05}$, and $ErCo_{1.8}Ni_{0.2}$.

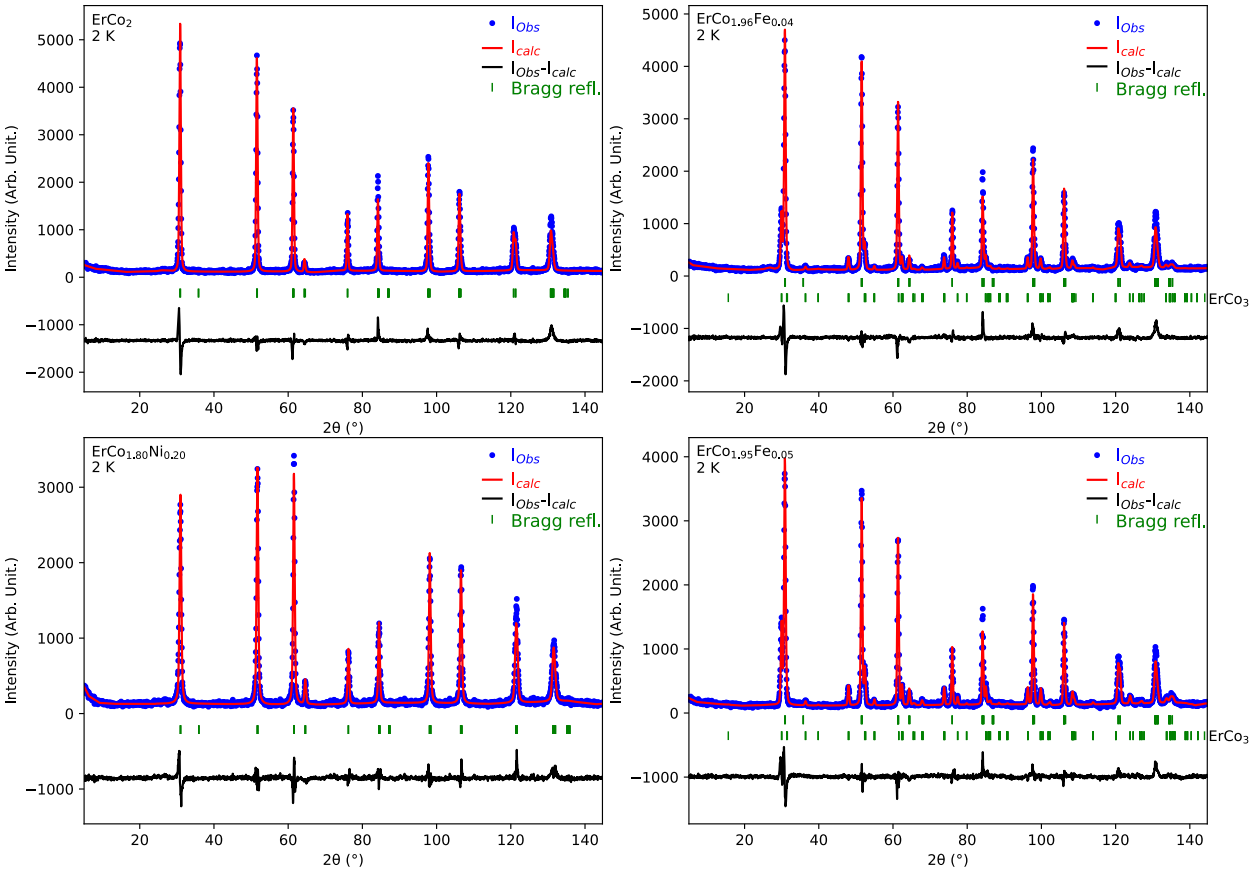

FIG. 2. Model refinements of NPD data gathered at 2 K for the $ErCo_2$, $ErCo_{1.96}Fe_{0.04}$, $ErCo_{1.95}Fe_{0.05}$, and $ErCo_{1.8}Ni_{0.2}$ samples.

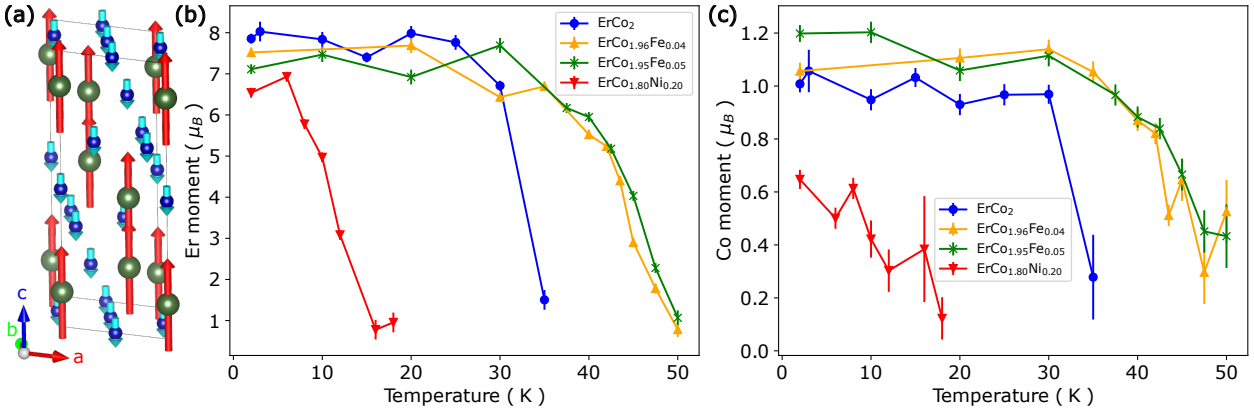

FIG. 3. (a) Visualization of the ferrimagnetic structure of $ErCo_2$. (b) Size of the Er moments extracted from Rietveld model refinements. (c) Size of the Co moments extracted from the Rietveld model refinements.

TABLE I. Refinement parameters achieved and phase fractions extracted from the model refinements of the neutron diffraction patterns.

	$ErCo_2$	$ErCo_{1.96}Fe_{0.04}$		$ErCo_{1.95}Fe_{0.05}$		$ErCo_{1.80}Ni_{0.20}$
Type	$ErCo_2$	$ErCo_2$	$ErCo_3$	$ErCo_2$	$ErCo_3$	$ErCo_2$
Space group	$Fd\bar{3}m$ (227)	$Fd\bar{3}m$ (227)	$R\bar{3}m$ (166)	$Fd\bar{3}m$ (227)	$R\bar{3}m$ (166)	$Fd\bar{3}m$ (227)
Temperature (K)	100	250		250		250
a (Å)	7.140(1)	7.1540(5)	4.9881(8)	7.1534(1)	4.9837(5)	7.144(1)
c [$ErCo_3$](Å)			24.263(9)		24.264(7)	
Volume (Å^3)	363.9(1)	366.13(5)	522.8(2)	366.04(1)	521.9(2)	364.63(9)
Phase(%)		85(1)	15(1)	79(2)	21(1)	
χ^2	1.70	1.64		1.81		1.57
Space group	$R\bar{3}m$ (166)	$R\bar{3}m$ (166)	$R\bar{3}m$ (166)	$R\bar{3}m$ (166)	$R\bar{3}m$ (166)	$R\bar{3}m$ (166)
Temperature (K)	2	2		2		2
a (Å)	5.0605(1)	5.0612(1)	4.9866(4)	5.0603(1)	4.9825(3)	5.0465(1)
c (Å)	12.3454(7)	12.3496(7)	24.273(5)	12.3491(7)	24.272(4)	12.327(1)
Volume (Å^3)	273.81(2)	273.97(2)	522.7(1)	273.85(2)	521.82(9)	271.87(3)
Phase(%)		85(3)	15(1)	79(2)	21(1)	
Er z	0.1263(6)	0.1268(6)		0.1269(6)		0.1261(7)
Er moment (μ_B)	7.9(1)	7.5(1)		7.1(1)		6.5(1)
Co moment (μ_B)	1.01(3)	1.05(3)		1.19(3)		0.65(4)
χ^2	3.95	4.11		3.47		2.96

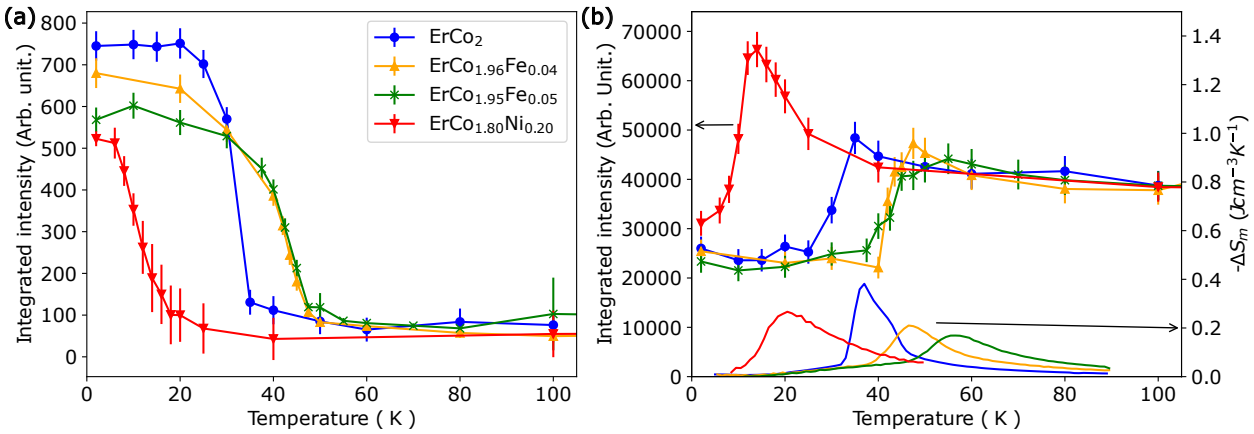

FIG. 4. Temperature dependencies of (a) the integrated intensities of the main magnetic reflection at 30° extracted by Gaussian fitting, and (b) the integrated intensities below 13.5° in 2θ for the various samples compared to the previously measured entropy change [7].

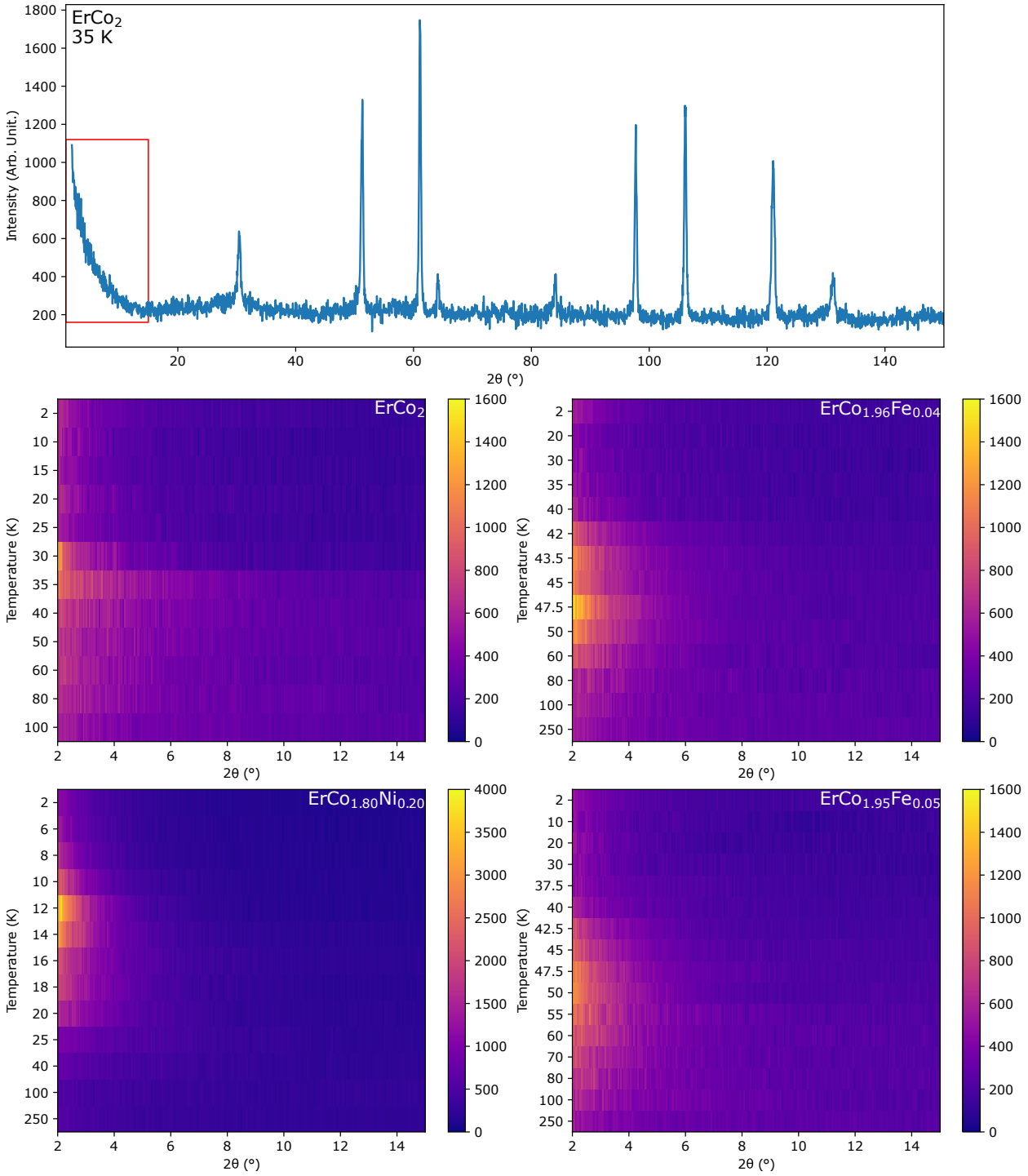

FIG. 5. The top part of the Figure shows the region displayed in the lower Figures. The middle and bottom part of the Figure shows the temperature dependence of the low angle region of the neutron powder diffraction patterns used to investigate the short range order.

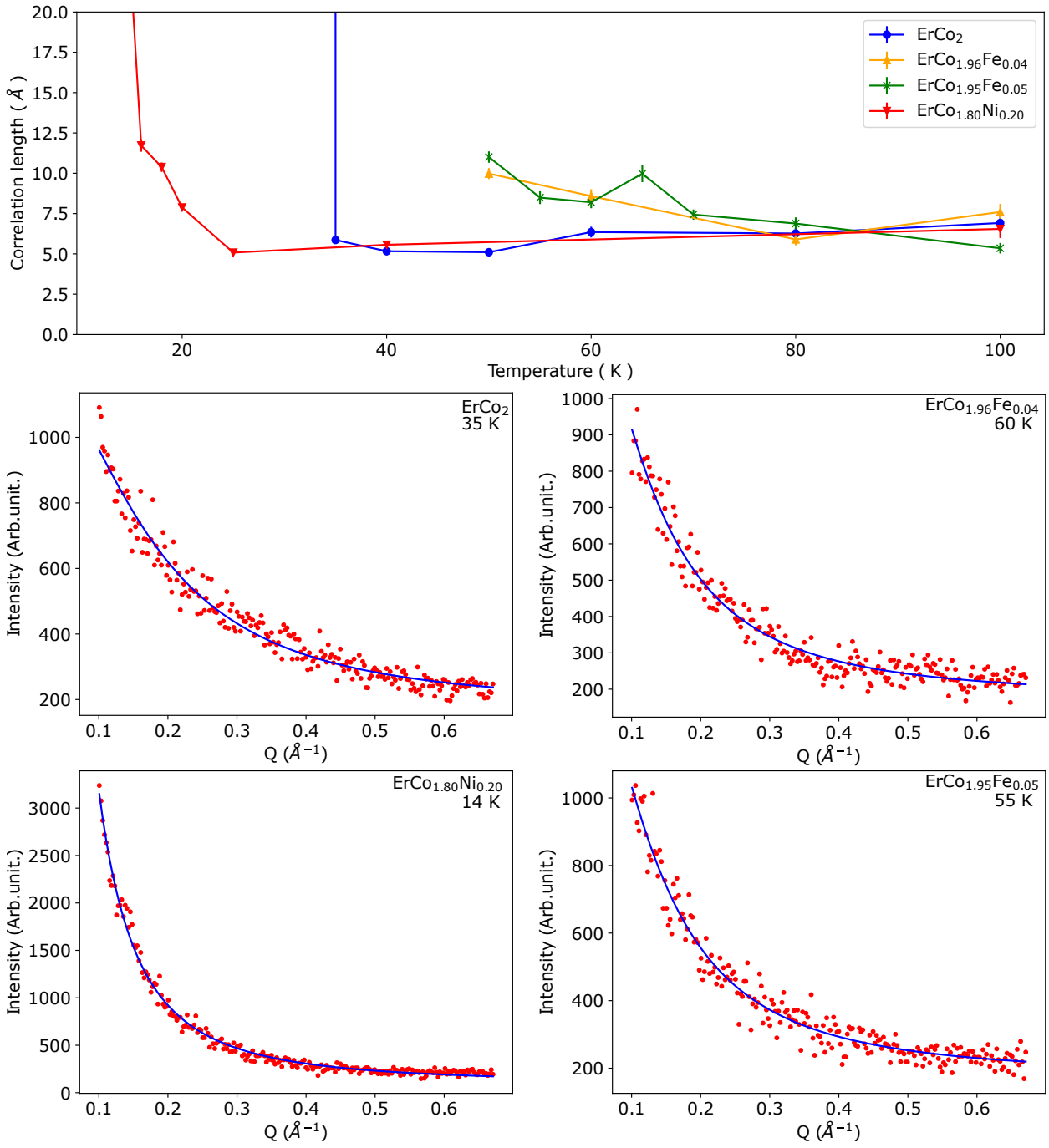

FIG. 6. Top part show the correlation lengths of the samples at various temperatures, which were extracted by modeling the 2 to 13.5 ° region of the diffraction patterns. Below are the fits of the low angle region in Q space for the each sample at the temperatures just prior to the onset of long range order.

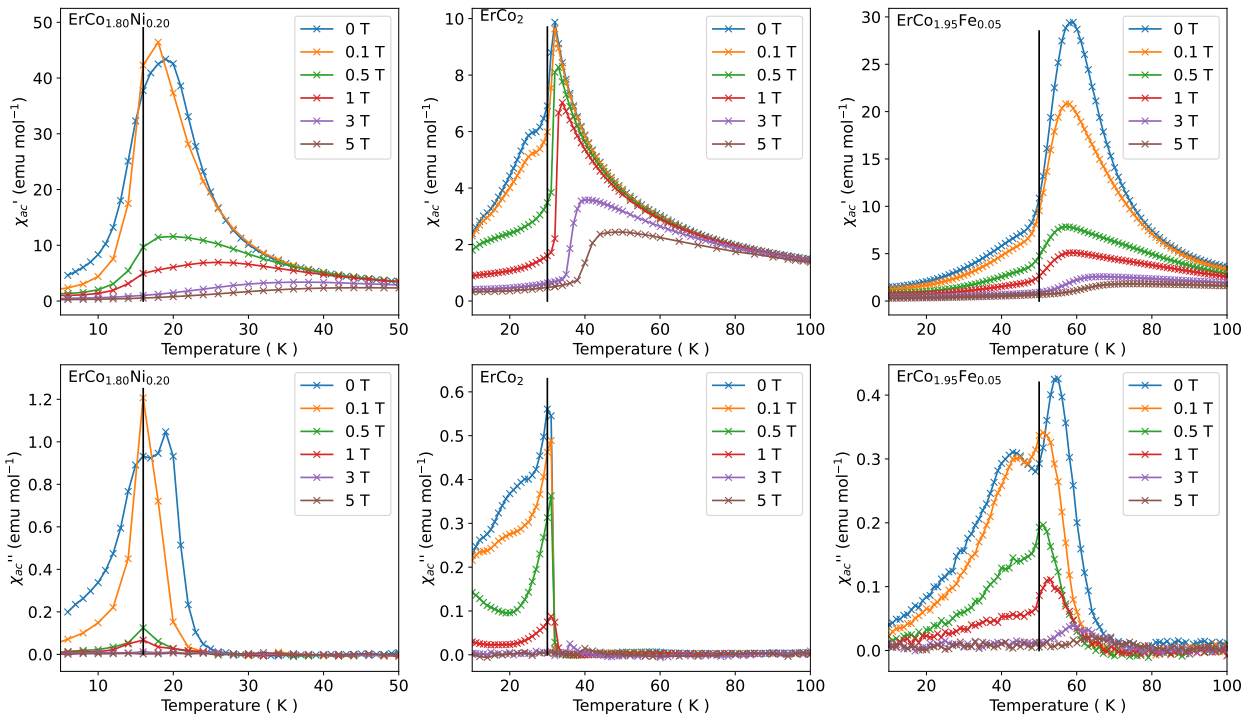

FIG. 7. Development of dynamic susceptibility components for $ErCo_{1.80}Ni_{0.20}$, $ErCo_2$, and $ErCo_{1.95}Fe_{0.05}$, under the influence of an applied field. The AC field was 56 Hz, but similar behavior was observed for other frequencies. The black vertical line denotes the T_C.

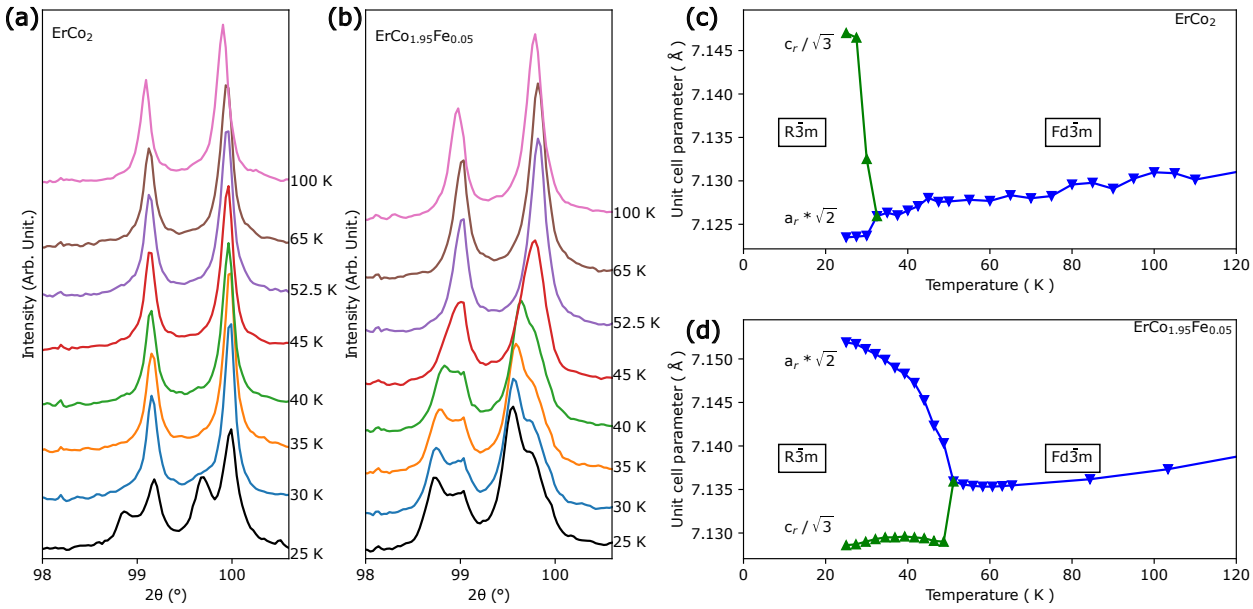

FIG. 8. Cubic to rhombohedral peak splitting seen in the XRPD data of (a) $ErCo_2$ and (b) $ErCo_{1.95}Fe_{0.05}$. The patterns have been offset for better readability. The difference in intensity of the Fe substituted sample compared to $ErCo_2$ is due differences in how the unit cell expands. (c)(d) The unit cell parameters extracted from the model refinements of $ErCo_2$ and $ErCo_{1.95}Fe_{0.05}$ respectively. The rhombohedral unit cell parameters have been transformed into their cubic unit cell equivalents.

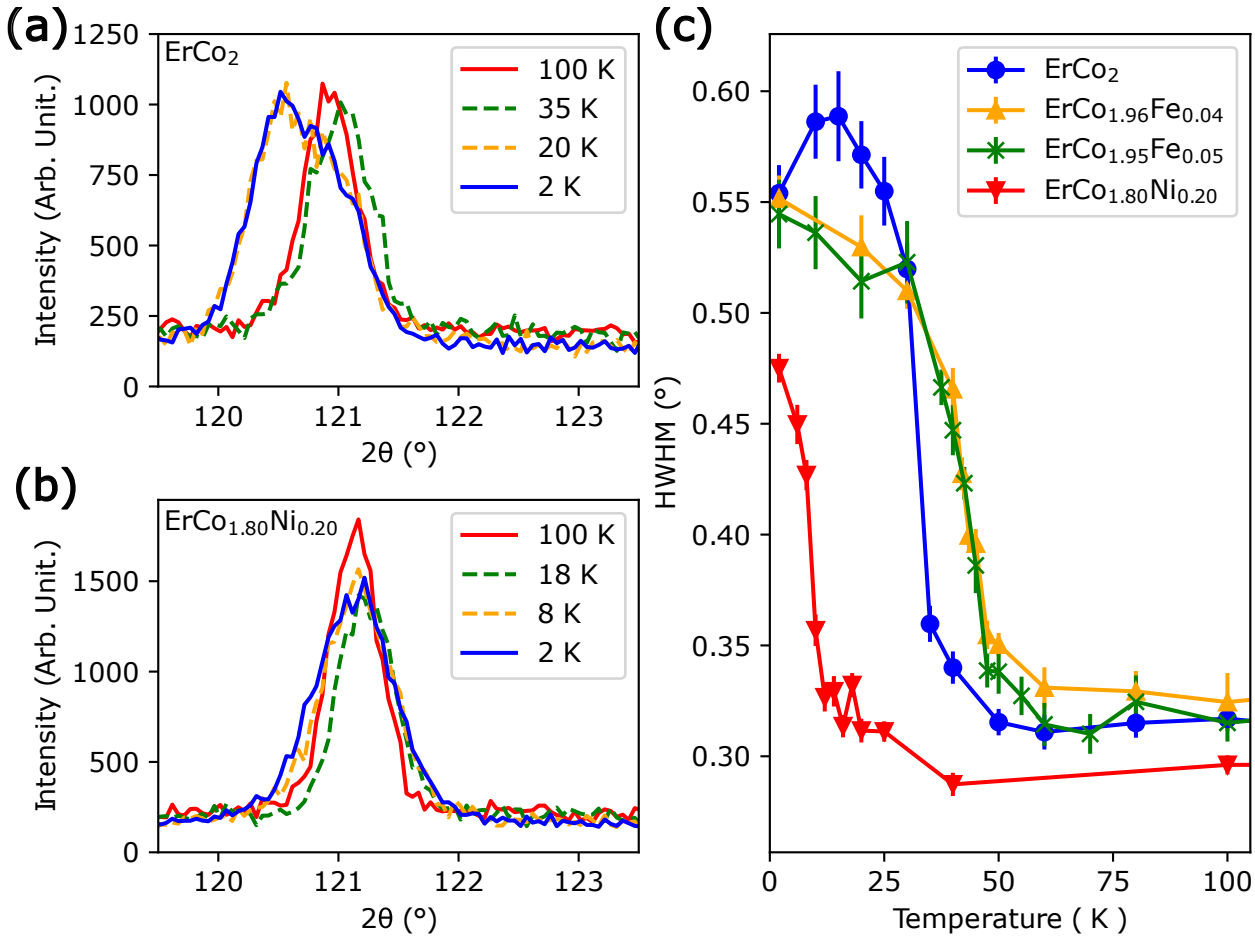

FIG. 9. The broadening of the cubic *440* reflection seen at 121° in the NPD data for (a) $ErCo_2$ and (b) $ErCo_{1.80}Ni_{0.20}$. Patterns have been normalized to the total neutron count of the 2 K data. (c) The temperature dependence of the broadening of the cubic (*440*) reflection for all samples.

TABLE II. Refinement parameters achieved and phase fractions extracted from the model refinements of the X-ray diffraction patterns.

	$ErCo_2$	$ErCo_{1.96}Fe_{0.04}$		$ErCo_{1.95}Fe_{0.05}$		$ErCo_{1.80}Ni_{0.20}$
Type	$ErCo_2$	$ErCo_2$	$ErCo_3$	$ErCo_2$	$ErCo_3$	$ErCo_2$
Space group	$Fd\bar{3}m$ (227)	$Fd\bar{3}m$ (227)	$R\bar{3}m$ (166)	$Fd\bar{3}m$ (227)	$R\bar{3}m$ (166)	$Fd\bar{3}m$ (227)
Temperature (K)	300	300		300		300
a (Å)	7.14836(6)	7.14940(6)	4.9917(6)	7.15150(6)	4.9921(4)	7.14036(7)
c [$ErCo_3$](Å)			24.193(1)		24.222(4)	
Volume (Å^3)	365.274(5)	365.434(5)	522.05(3)	365.756(6)	522.8(1)	364.049(6)
Phase(%)	96.1(3)	95.0(3)	3.3(2)	85.3(3)	11.1(2)	97.4(3)
χ^2	13.70	16.40		9.80		26.80
Space group	$R\bar{3}m$ (166)	$R\bar{3}m$ (166)	$R\bar{3}m$ (166)	$R\bar{3}m$ (166)	$R\bar{3}m$ (166)	$Fd\bar{3}m$ (227)[a]
Temperature (K)	25	25		25		25
Magnetism	Ferri	Ferri	Ferri	Ferri	Ferri	Para
a (Å)	5.03708(7)	5.05135(5)	4.9866(4)	5.05716(6)	4.9889(3)	7.11817(5)
c (Å)	12.3789(3)	12.3366(3)	24.273(5)	12.3471(3)	24.222(3)	
Volume (Å^3)	272.001(9)	272.609(7)	520.3(5)	273.470(8)	522.10(8)	360.666(4)
Phase(%)	96.3(3)	95.9(4)	2.4(2)	84.2(4)	13.5(2)	97.6(3)
Er z	0.1260(2)	0.1242(2)		0.1256(2)		
χ^2	17.00	21.60		28.40		37.00

[a] $ErCo_{1.80}Ni_{0.20}$ is still in the paramagnetic cubic state at 25 K

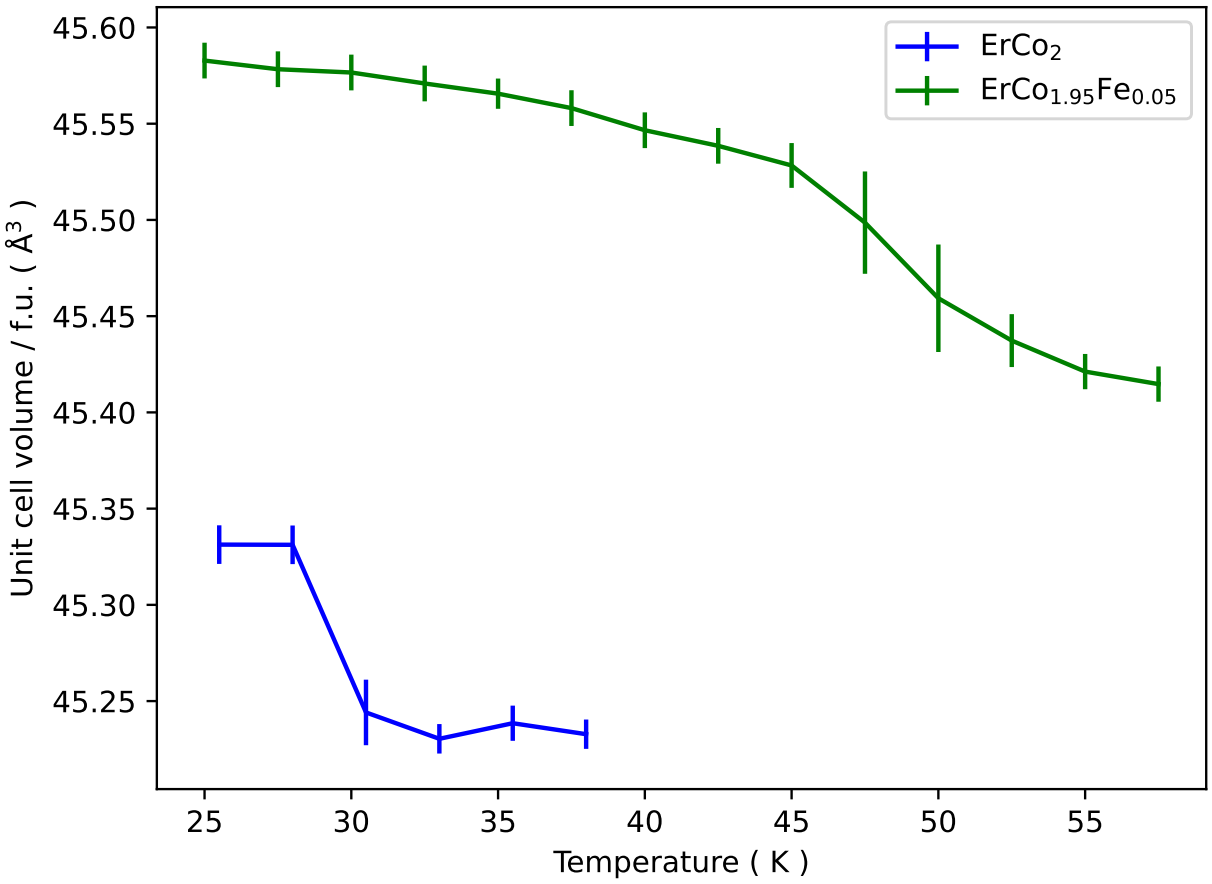

FIG. 10. The volume per formula unit of $ErCo_2$ and $ErCo_{1.95}Fe_{0.05}$ extracted from model refinements of the synchrotron XRPD patterns. The three points at the highest temperature for each sample has the cubic Laves configuration.

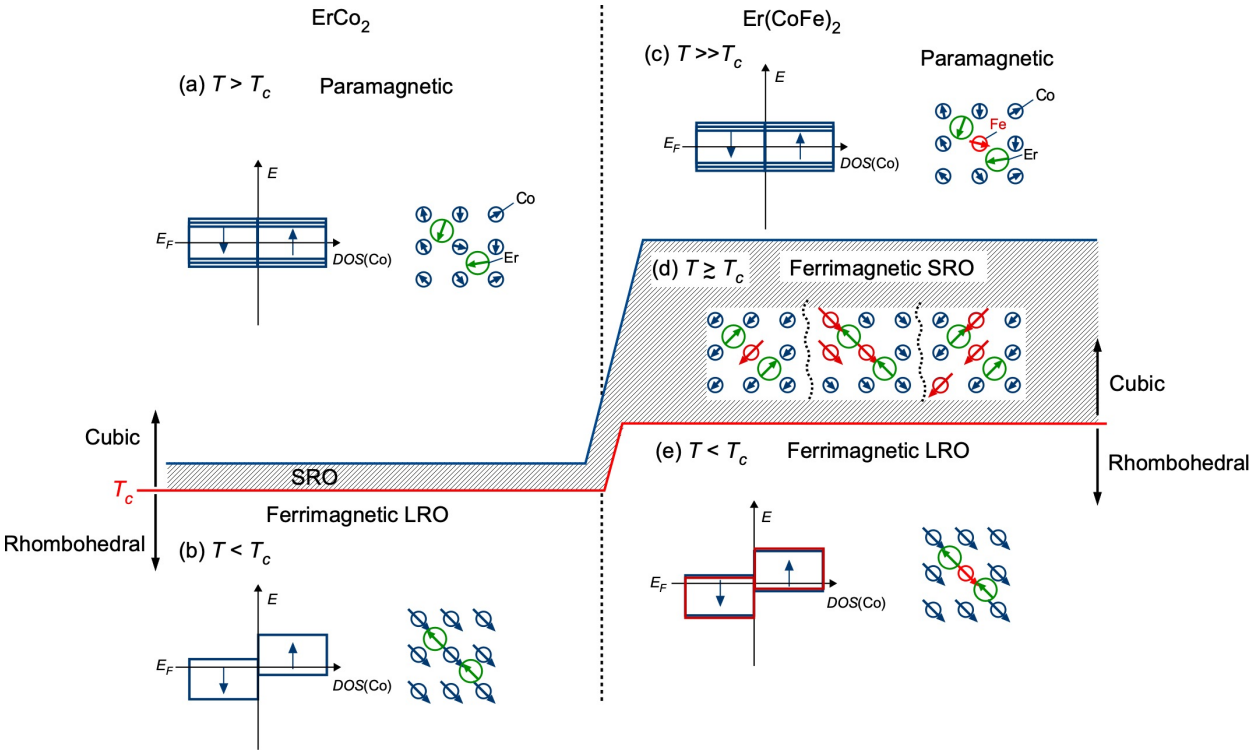

FIG. 11. Schematic drawings of magnetic orderings and the associated density of state (DOS) of Co in $ErCo_2$ and $Er(CoFe)_2$. (a)(c) represents the paramagnetic phase, and (b)(e) represents the low temperature ferrimagnetic phase. (d) describes the ferrimagnetic short range order in the intermediate temperature region in $Er(CoFe)_2$.